Sundararaman, A., Fukushima, Y., Norman, J. C., Uemura, A., & Mellor, H. (2020). RhoJ regulates α5β1 integrin trafficking to control fibronectin remodeling during angiogenesis. *Current Biology*, *30*, P2146-2155. https://doi.org/10.1016/j.cub.2020.03.042

RhoJ regulates α5β1 integrin trafficking to control fibronectin remodeling during angiogenesis

Ananthalakshmy Sundararaman[1], Yoko Fukushima[2], Jim C. Norman[3], Akiyoshi Uemura[4] and Harry Mellor[1,*]

[1] School of Biochemistry, Biomedical Sciences Building, University of Bristol, Bristol BS8 1TD, UK
[2] Department of Ophthalmology, Osaka University Graduate School of Medicine, Suita, Japan
[3] CRUK Beatson Institute for Cancer Research, Garscube Estate, Glasgow G61 1BD, UK
[4] Department of Retinal Vascular Biology, Nagoya City University Graduate School of Medical Sciences, 1 Kawasumi Mizuho-cho, Mizuho-ku, Nagoya 467-8601, Japan

Email contacts:

AS: as16502@bristol.ac.uk
YF: yokofukushima@icloud.com
JCN: j.norman@beatson.gla.ac.uk
AU: uemura@med.nagoya-cu.ac.jp
HM: h.mellor@bristol.ac.uk

* Lead Contact and Corresponding Author: Professor Harry Mellor

SUMMARY

Rho GTPases are master regulators of cell shape and cell movement [1]. The archetypal family members RhoA, Rac1 and Cdc42 arose early in eukaryotic evolution and coordinate a diverse range of cell morphologies and migrations. Evolution of the vertebrates was paralleled by expansion of this family through gene duplication. Emergence of an adaptive immune system and more complex neural systems presented new roles for Rho GTPases, filled by new family members. Cdc42 underwent gene duplication to produce two related proteins – RhoQ and RhoJ [2]. RhoQ is active in neural dynamics; however, RhoJ is highly expressed in endothelial cells under control of the endothelial-specific promoter ERG [3, 4]. RhoJ is required for angiogenesis [5, 6] and has multiple roles in this process [7, 8]. We recently demonstrated that RhoJ regulates the endosomal trafficking of podocalyxin during angiogenesis to control lumen formation [9]. Here we use vesicle purification and proteomic analysis to identify the endothelial targets of RhoJ-mediated trafficking. We identify α5β1 integrin as a major RhoJ cargo and show that RhoJ regulates the intracellular trafficking of active α5β1 integrin in endothelial cells to repress fibronectin fibrillogenesis. Accordingly, mice lacking RhoJ show deregulated deposition of fibronectin around vessels during developmental angiogenesis. Intriguingly, we show that RhoJ acts in opposition to Cdc42 in this process through competition for a shared partner, PAK3. These studies identify a critical role for RhoJ in matrix remodeling during blood vessel formation and demonstrate a functional interrelationship between RhoJ and its evolutionary parent.

Keywords: endothelial, Rho GTPase, fibrillogenesis, angiogenesis, integrin, intracellular traffic

RESULTS AND DISCUSSION

Endothelial RhoJ+ vesicles transport α5β1 integrin

Cdc42 and RhoJ are both required for angiogenesis [5, 10], suggesting that these related proteins have discrete functions in the process. The most immediately apparent difference between the two is in their localization. In primary human endothelial cells (ECs) we observed a broad cytoplasmic distribution for Cdc42, whereas RhoJ also localized to a vesicular pool (Figure 1A). RhoJ was first identified as an endosomal Rho GTPase [11], and accordingly these vesicles colocalized with the early endosomal marker EEA1 and the late endosomal/lysosomal marker LAMP1 (Figures 1A, S1A). We purified these vesicles to determine their content. Primary ECs were transduced with GFP-tagged RhoJ and the cells broken mechanically. Cellular membranes were fractionated by centrifugation on iodixanol density gradients. RhoJ was detected in plasma membrane fractions and in the early and late endosomal fractions (Figure 1B). We pooled the vesicular RhoJ fractions and further purified these by particle sorting. The membrane fractions were incubated with Calcein Violet to label sealed vesicles [12] and dual-sorted to derive a homogenous GFP-RhoJ+ vesicle population (Figure 1C). The protein content was then determined by mass spectrometry. In keeping with their identity, RhoJ+ vesicles were marked by a subset of endosomal Rab GTPases (Figure 1D, Data S1). Intriguingly, the cargo of RhoJ+ vesicles was enriched in cell adhesion proteins, including both integrins, EC adhesion molecules and also desmosome components (Figure 1D; Data S1). The most abundant integrin was α5β1, which is required for both normal developmental angiogenesis and for tumor angiogenesis [13, 14]. Staining of ECs for endogenous α5 and β1 integrin subunits revealed strong colocalization with RhoJ+ vesicles (Figure 1E). The colocalization with α5 was greater than with β1 (78% versus 52%; Figure 1E). β1 integrin is part of multiple integrin dimers in ECs, whereas α5 is only found in the α5β1 complex [15]. We examined the localization of three other adhesion proteins from the RhoJ vesicle proteome – PECAM, VE-cadherin and α2 integrin (Figure S1B). All showed colocalization with RhoJ in vesicles, although to a lesser degree than α5β1 integrin (Figure S1B). We conclude that α5β1 integrin is a major cargo of RhoJ+ vesicles in ECs.

RhoJ regulates trafficking of active endothelial α5β1 integrin

Integrin trafficking is critical to integrin function. Integrins from disassembled adhesions must be endocytosed and then recycled to new adhesive sites to allow for dynamic morphology and migration [16, 17]. We were interested to see if RhoJ regulated α5β1 trafficking. As α5 is only found in the α5β1 complex [15], we examined α5 localization as a surrogate for α5β1 integrin. Silencing of RhoJ (Figure 2A) had no effect on the cellular distribution of total α5 integrin, as judged by immunofluorescence microscopy (Figure 2B), or density gradient fractionation (Figure S2A). Similarly, expression of an activated RhoJ-QL mutant had no apparent effect on the distribution of total α5 integrin (Figures 2B, S2C). The SNAKA51 antibody is specific for the extended conformation of the α5β1 complex [18] and consequently recognizes α5β1 in its activated form in fibrillar adhesions [19]. Silencing of RhoJ significantly increased SNAKA51 staining in ECs, consistent with an increase in activation of α5β1 integrin (Figure 2C). In contrast, expression of activated RhoJ significantly reduced SNAKA51 staining (Figure 2C). We isolated α5β1 from ECs by immunoprecipitation with either total α5 integrin antibody or

SNAKA51. Silencing of RhoJ had no effect on total levels of α5β1 (Figure S2B), but significantly increased the proportion of activated integrin (Figure 2D). Conversely, activated RhoJ dramatically reduced levels of activated α5β1 (Figure 2E), without affecting total α5β1 levels (Figure S2C).

Silencing of RhoJ increased SNAKA51 staining at fibrillar adhesions and also seemingly in vesicles (Figure 2C). We found that permeabilization of ECs with saponin allowed selective visualization of the vesicular pool, facilitating its quantification. RhoJ silencing significantly increased the number of SNAKA51+ vesicles (Figure S2D), suggesting increased uptake of the activated integrin. We examined this using an internalization assay. Surface proteins were biotinylated on ice and then allowed to internalize following a shift to 37°C. At each time point, cells were treated to remove surface biotinylation and the remaining (internalized) biotinylated protein was captured. Levels of internalized α5β1 were quantified by ELISA. Silencing of RhoJ had no significant effect on the endocytosis of total α5β1 (Figure 2F) in keeping with the lack of effect on cellular localization of total α5β1 (Figures 2B, S2A). In contrast, silencing of RhoJ significantly increased the internalization of active α5β1 (Figure 2F). In the assay, internalized active α5β1 will eventually resolve through the recycling and degradative pathways. Silencing of RhoJ also increased amount of internalized active α5β1 present at later time points (Figure 2F), suggesting that RhoJ also affects the subsequent onward trafficking of this complex. Recent work has shown that active α5β1 recycles via a TGN46+ compartment in ECs [20]. We examined the steady-state distribution of active α5β1 in ECs and found that loss of RhoJ significantly increased the pool of active α5β1 in TGN46+ recycling vesicles, with a parallel reduction in vesicles positive for the late endosomal/lysosomal marker LAMP1 (Figures 2G, S2E). To examine this further, we performed recycling assays. In these assays, the fate of a pool of internalized, biotinylated α5β1 is followed over time. While silencing of RhoJ increased the presence of active α5β1 in the TGN46+ recycling compartment, it had no significant effect on the rate of return of active integrin to the cell surface (Figure 2H). The rate of recycling of total α5β1 was not affected either (Figure 2H).

We conclude that RhoJ suppresses an internalization pathway that carries active α5β1 to the TGN46+ recycling pathway. In the absence of RhoJ, more active α5β1 heterodimers are internalized. While the rate of return of active α5β1 is unaffected, the size of the internal pool is increased and so the amount of active α5β1 returned to the surface is greater. Depletion of RhoJ also causes a shift in the localization of internalized active α5β1 away from the late endosomal compartment and towards the TGN46+ recycling compartment, suggesting that RhoJ may alter the route of trafficking also.

α2β1 is an important collagen receptor in ECs [15]. As we identified α2 integrin in the RhoJ vesicle proteome (Figure 1D), we examined whether RhoJ also regulates trafficking of this integrin. Depletion of RhoJ caused a small increase in the internalization of α2 integrin but did not affect its recycling rate (Figure S2F), or the distribution of α2 integrin between the surface and internal pools (Figure S2G). Tools are not available to measure the trafficking of active α2β1 and so we cannot exclude a role for RhoJ in trafficking of the active α2β1 integrin.

RhoJ regulates the endothelial assembly of fibrillar fibronectin

RhoJ has been shown to regulate the size and number of focal adhesions in ECs [3], suggesting a possible role for RhoJ in mediating EC adhesion. Integrin α5β1 is the major receptor for fibronectin in ECs [21], so we compared adhesion to fibronectin with other ECM components. Silencing of RhoJ had a small but significant inhibitory effect on EC adhesion, but not specifically to fibronectin (Figure S3A). Similarly, activated RhoJ increased general adhesion to a small but significant degree (Figure S3A). Integrin α5β1 is also critical for the remodeling of secreted soluble fibronectin into fibrillar fibronectin [22]. ECs assemble fibrillar fibronectin during angiogenesis and this temporary 3D matrix is required for vessel formation [23]. Fibronectin fibrillogenesis requires the internalization and recycling of active α5β1 integrin through the TGN46+ compartment [20, 24, 25], suggesting that active RhoJ might inhibit this process. Indeed, silencing of RhoJ led to a dramatic increase in the assembly of fibronectin into fibrils that was apparent both visually (Figure 3A) and in the quantification of deoxycholate-insoluble fibronectin fibrils (Figure 3B). Conversely, expression of activated RhoJ suppressed fibronectin fibrillogenesis (Figures 3A, 3C). Identical results were obtained with exogenously added, fluorescent fibronectin, demonstrating that this does not depend on fibronectin synthesis (Figure S3B). Similarly, RhoJ did not affect the rate of secretion of fibronectin from ECs (Figure S3C), demonstrating that this effect was not due to a net increase in fibronectin production by the cells. We conclude that RhoJ negatively regulates the assembly of soluble fibronectin into fibrils.

RhoJ opposes Cdc42 in regulating fibronectin fibrillogenesis through competition for PAK3

Recent work has shown that RhoJ and Cdc42 are reciprocally regulated in ECs. Cdc42 is activated by the pro-angiogenic growth factor VEGF downstream of Arhgef15, whereas RhoJ is inactivated [26]. Conversely, the guidance molecule semaphorin 3E activates RhoJ in ECs during angiogenesis and inhibits Cdc42 [27]. This evidence for reciprocal regulation suggested that some functions of these Rho GTPases might be in opposition. Accordingly, we found that silencing of Cdc42 (Figure S3D) significantly inhibited fibronectin fibrillogenesis (Figures 3D, 3E), whereas activated Cdc42 promoted this process (Figures 3D, 3F).

RhoJ is known to have an overlapping binding specificity with Cdc42 and to share partners such as WASP and PAK1 [11, 28]. To identify RhoJ/Cdc42 binding partners in ECs, we transduced cells with GFP-tagged, activated mutants of the two proteins and analyzed the complexes by tandem mass-tag mass spectrometry [29]. The majority of known Cdc42 interactors could also be found in RhoJ complexes (Figure 4D, Data S2). Interestingly, RhoJ appeared to interact less well overall, and bound to some Cdc42 effectors better than others (Figure 4D). Of the previously characterized Cdc42 interactors, RhoJ bound best to PAK3 in ECs (Figure 4D). This interaction was confirmed by immunoprecipitation (Figure S3E). In keeping with the mass spectrometry data, Cdc42 was more effective at immunoprecipitating PAK3, suggesting a higher binding efficiency (Figure S3E). Silencing of PAK3 (Figure S3F) had no effect on the rate of internalization of active α5β1, but like RhoJ caused an increase in amount of internalized activated integrin in the cell at later timepoints (Figure S3I).

The effects of silencing of PAK3 on fibronectin fibrillogenesis phenocopied the effects of silencing of Cdc42, with significant loss of fibrillar fibronectin (Figures 4A, 4B). Similarly, overexpression of PAK3 phenocopied Cdc42 activation, with promotion of fibrillogenesis (Figures 4A, 4C). There was no change to the rate of fibronectin secretion (Figure S3H). Intriguingly, activated RhoJ was able to suppress the promotion of fibrillogenesis caused by PAK3 and, by corollary, PAK3 was able to partially rescue the inhibition of fibrillogenesis caused by activated RhoJ (Figure 4E, S3G). We conclude that RhoJ negatively regulates fibronectin fibrillogenesis in ECs at least in part by competition with Cdc42 for PAK3.

PAK3 is related to PAK1 and 3; collectively forming the Group I PAKs [30]. Silencing of PAK2 did not affect fibrillogenesis; however, silencing of PAK1 did, although to a lesser degree than PAK3 (Figures S4A-C). Interestingly, RhoJ has previously been shown to activate PAK1 and PAK3 in melanoma cells, but not PAK2 [31]. Treatment of ECs with the Group I PAK inhibitor FRAX486 had a greater effect than silencing either PAK alone (Figure S4D), suggesting that both PAK1 and PAK3 contribute to this process.

RhoJ regulates fibronectin fibrillogenesis during angiogenesis

To determine the role of RhoJ in fibronectin fibrillogenesis *in vivo*, we examined fibronectin deposition during developmental angiogenesis of the retina in RhoJ -/- mice. RhoJ is highly expressed in the ECs of these vessels as they develop [4, 27] and loss of RhoJ causes a reduced rate of vessel outgrowth that is associated with destabilization of new capillaries at the vascular front [4]. At postnatal day 7, modest deposition of fibronectin was detected broadly over the developing retinal vasculature in wild-type mice (Figures 4F, S4E). In contrast, loss of RhoJ led to a marked increase in fibronectin staining specifically at the vascular front, with the additional fibronectin wrapped around the actively forming vessels (Figures 4F, S4E). We conclude that RhoJ functions in angiogenesis to control the deposition of the fibrillar fibronectin matrix, with a loss of this function leading to instability and regression of newly formed vessels due retention of this provisional matrix.

Our work has uncovered a key role for RhoJ in the trafficking of active α5β1 integrin. Active β1 integrins are trafficked differently to inactive β1 integrins, with a higher internalization rate and sorting to the late endosomal compartment prior to recycling [32]. RhoJ acts to inhibit internalization of the active form of α5β1 specifically, leading to decreased flux through the cell. While RhoJ does not affect the rate of recycling of internalized, active α5β1, it appears to route it away from the TGN46+ compartment and towards the late endosomal compartment. As traffic through the TGN46+ compartment is required for fibronectin fibrillogenesis [20], the net effect is to decrease the supply of active α5β1 for this process.

ECs assemble fibrillar fibronectin during angiogenesis to provide a provisional proangiogenic matrix for vessel formation [23]. Conversely, fibrillogenesis must be switched off in mature vessels to promote stability and to avoid generation of pro-inflammatory, atherogenic signals. Our data support a model (Graphical Abstract) in which RhoJ suppresses fibronectin fibrillogenesis in quiescent ECs. At the onset of angiogenesis, VEGF-mediated inactivation of RhoJ would then release this brake, allowing for deposition of the provisional fibronectin matrix.

RhoJ would then be reactivated at the end of vessel formation to allow its role in lumenogenesis [9]. Importantly, RhoJ reactivation would also suppress fibronectin deposition in the mature vessel, allowing for stability and a return to quiescence. It is apparent that VEGF receptor signaling acts on integrin function in many ways in ECs [33, 34] and it will be important to explore the links between these pathways and RhoJ signaling in further detail.

The discovery of reciprocal roles for RhoJ and Cdc42 in this process also gives insight into the functional consequences of the expansion of the Rho GTPase family. We had expected to find unique RhoJ partners that would mediate the specific roles of RhoJ in the endothelium. Instead we found that RhoJ interacts with a largely overlapping set of partners to Cdc42, albeit with a different order of preference. RhoJ acts in opposition to its more ancient relative Cdc42, competing for their shared partner PAK3. In this way, the reciprocal regulation of these two Rho GTPases during angiogenesis allows for reciprocal regulation of fibrillogenesis. Similar gene duplications have occurred for Rac1 and RhoA, the two other archetypal Rho GTPases. It will be important to determine if similar reciprocal regulatory mechanisms exist elsewhere in the Rho GTPase family.

ACKNOWLEDGEMENTS

The authors thank Professor Martin Schwartz for invaluable discussion and advice.
We thank Dr Kate Heesom of the University of Bristol Proteomic Facility for proteomic analysis and Drs Andy Herman and Lorena Sueiro Ballesteros of the University of Bristol Flow Facility for assistance with particle sorting. The study was supported by project grant PG/16/62/32295 from the British Heart Foundation.

AUTHOR CONTRIBUTIONS

Conceptualization, A.S and H.M.; Methodology, A.S., H.M., J.C.N. and A.U.; Investigation, A.S., J.C.N and Y.F.; Writing – Original Draft, H.M.; Writing – Review & Editing, A.S., Y.F., J.C.N. and A.U.; Funding Acquisition, H.M.; Resources, J.C.N., A.U. and H.M.; Supervision, J.C.N., A.U. and H.M.

DECLARATION OF INTERESTS

The authors declare no competing interests.

FIGURE LEGENDS

Figure 1. Endothelial RhoJ+ vesicles transport α5β1 integrin

(A) ECs were transfected with GFP-Cdc42 or GFP-RhoJ. Cdc42 had a broad cytoplasmic distribution, whereas RhoJ was also seen in vesicles that colocalized with the early endosomal marker EEA1 (red). Quantification of these vesicles showed substantial colocalization with EEA1 and with the late endosomal marker LAMP1 (Figure S1A), but not with the trans-Golgi marker TGN46. Data are means ± SEM; n=10 cells. Scale bar = 10μm.

(B) Post-nuclear supernatants from ECs transduced with GFP-RhoJ QL were subjected to density ultracentrifugation on 10-30% iodixanol gradients. Fractions were analyzed by western blotting. RhoJ was recovered in membranes co-sedimenting with the plasma membrane marker Na^+/K^+ ATPase, and with the early endosomal maker EEA1 and the late endosomal marker CD63. Lesser amounts co-sedimented with the lysosomal marker LAMP2 or the endoplasmic reticulum marker calnexin.

(C) RhoJ+ endosomes from the density gradient (blue box; Panel B) were post-labelled with Calcein Violet and further purified by particle sorting. Purified RhoJ+ vesicles were analyzed by mass spectrometry.

(D) The RhoJ+ vesicle proteome (see Data S1) was filtered for a 1% false discovery rate and manually annotated into functional categories. The pie chart shows the major classes of proteins present. The RhoJ+ vesicle proteome was enriched in metabolic enzymes, cytoskeletal proteins and trafficking proteins. Transmembrane proteins were annotated as vesicle 'cargo', of which 45% were cell adhesion proteins. The Table shows individual adhesion proteins and Rab GTPases identified in the proteome.

(E) ECs were transfected with GFP-RhoJ and co-stained for endogenous α5 and β1 integrins (red). RhoJ+ vesicles colocalized with both α5β1 subunits. Scale bar = 10μm. Data are means ± SEM; n=10 cells.

Figure 2. RhoJ regulates active integrin α5β1 trafficking

(A) ECs were transfected with two independent RhoJ siRNAs and the effectiveness of silencing determined by western blotting.

(B) The cellular distribution of α5 integrin was determined by immunofluorescence microscopy. Neither silencing of RhoJ, or expression of an active RhoJ QL mutant affected α5 integrin distribution (see also Figure S2A). Scale bar = 10μm.

(C) The cellular distribution of active α5β1 was examined in ECs using the conformation-specific SNAKA51 antibody. Silencing of RhoJ significantly increased SNAKA51 staining intensity, whereas expression of the intensity activated RhoJ QL significantly reduced it. Scale bar = 10μm. The graphs present quantification of active α5β1 staining, relative to control cells. Data are means ± SEM; n=9 independent experiments. *** $P \leq 0.001$; ** $P \leq 0.01$; * $P \leq 0.05$.

(D) ECs were treated ± RhoJ siRNA. Total and active α5β1 integrin were isolated separately by immunoprecipitation and quantified by western blotting. Silencing of RhoJ had no effect on total α5β1 integrin levels (see Figure S2B); however, quantification showed a significant increase in levels of active α5β1 (Data are means ± SEM; n=3 independent experiments). * $P \leq 0.05$.

(E) ECs were transduced with RhoJ QL and total and active α5β1 integrin were isolated separately by immunoprecipitation and quantified by western blotting. Expression of activated RhoJ had no effect on total α5β1 integrin levels (see Figure S2C); however, quantification showed a significant decrease in levels of active α5β1. Data are means ± SEM; n=3 independent experiments. ** $P \leq 0.01$.

(F) ECs were treated ± RhoJ siRNA. After 72h, cells were surface biotinylated on ice and then allowed to internalize surface proteins at 37°C. At each timepoint, the remaining surface biotinylation was removed by MesNa treatment, and the amount of internalized α5β1 integrin was determined by streptavidin capture of biotinylated proteins and ELISA with α5β1 integrin-specific antibodies. Silencing of RhoJ had no significant effect on the internalization of total α5β1 integrin, but significantly increased the rate of internalization of active α5β1. At later timepoints, levels of internalized active α5β1 were preserved, suggesting there was also a change to onward trafficking. Data are means ± SEM; n=3 independent experiments. *** $P \leq 0.001$; ** $P \leq 0.01$; * $P \leq 0.05$.

(G) ECs were treated ± RhoJ siRNA. After 48h, the steady-state distribution active α5β1 integrin was determined by confocal immunofluorescence microscopy (see Figure S2E). Quantification showed that silencing of RhoJ significantly decreased the amount of active α5β1 integrin in LAMP1+ late endosomes/lysosomes and significantly increased the amount of active α5β1 integrin in TGN46+ vesicles, consistent with a switch towards recycling of the active integrin. Data are means ± SEM; n=4 independent experiments, 5 cells in each condition/experiment. **** $P \leq 0.0001$; *** $P \leq 0.001$; ** $P \leq 0.01$.

(H) ECs were treated ± RhoJ siRNA. After 72h, cells were surface biotinylated on ice and then allowed to internalize surface proteins at 37°C for 24min. Biotin on the remaining non-internalised receptors was then removed using MesNa on ice. The internalised pool was then chased over the time points indicated and the biotin from recycled receptors was again removed by reduction with MesNa on ice. The amount of internalised pool lost to the surface is represented as % of the initial internalised pool in each case. Silencing of RhoJ had no significant effect on the recycling rate for total or active integrin α5β1. Data are means ± SEM; n=3 experiments.

Figure 3: RhoJ regulates the endothelial assembly of fibrillar fibronectin

(A) ECs were treated ± RhoJ siRNA or transduced with RhoJ QL. Fibronectin deposition was examined by staining cells with an EDA-fibronectin antibody to detect cell-secreted fibronectin specifically. Scale bar = 10μm. Silencing of RhoJ significantly increased fibronectin fiber density, quantified as detailed in the methods. Conversely, expression of the activated RhoJ QL

mutant significantly decreased fiber density (means ± SEM; n≥4 independent experiments). See also Figure S3B. ** $P \leq 0.01$; * $P \leq 0.05$.

(B) Fibronectin fibrillogenesis in ECs was quantified by isolating deoxycholate (DOC) insoluble fibronectin and western blotting. Silencing of RhoJ significantly increased fibrillogenesis (means ± SEM; n=3 independent experiments). * $P \leq 0.05$.

(C) ECs were transduced with RhoJ QL and fibronectin fibrillogenesis was quantified by isolating DOC-insoluble fibronectin and western blotting. Expression of activated RhoJ significantly inhibited fibrillogenesis (means ± SEM; n=3 independent experiments). ** $P \leq 0.01$.

(D) ECs were treated ± Cdc42 siRNA or transduced with Cdc42 QL. Fibronectin deposition was examined by staining cells with an EDA-fibronectin antibody to detect cell-secreted fibronectin specifically. Scale bar = 10μm. Silencing of Cdc42 significantly decreased fibronectin fiber density. Conversely, expression of the activated Cdc42 QL mutant significantly increased fiber density (means ± SEM; n=4 independent experiments). ** $P \leq 0.01$; * $P \leq 0.05$.

(E) Fibronectin fibrillogenesis in ECs was quantified by isolating deoxycholate (DOC) insoluble fibronectin and western blotting. Silencing of Cdc42 (see Figure S3C) significantly decreased fibrillogenesis (means ± SEM; n=3 independent experiments). * $P \leq 0.05$.

(F) ECs were transduced with Cdc42 QL and fibronectin fibrillogenesis was quantified by isolating DOC-insoluble fibronectin and western blotting. Expression of activated Cdc42 significantly increased fibrillogenesis (means ± SEM; n=3 independent experiments). * $P \leq 0.05$.

Figure 4. RhoJ opposes Cdc42 in endothelial fibronectin fibrillogenesis through competition for PAK3

(A) ECs were treated ± PAK3 siRNA (see Figure S3F) or transduced with myc-tagged PAK3. Fibronectin deposition was examined by staining cells with an EDA-fibronectin antibody to detect cell-secreted fibronectin specifically. Scale bar = 10μm. Silencing of PAK3 significantly decreased fibronectin fiber density. Conversely, overexpression of PAK3 significantly increased fiber density (means ± SEM; n=4 independent experiments). *** $P \leq 0.001$; * $P \leq 0.05$.

(B) Fibronectin fibrillogenesis in ECs was quantified by isolating deoxycholate (DOC) insoluble fibronectin and western blotting. Silencing of PAK3 significantly decreased fibrillogenesis (means ± SEM; n=3 independent experiments). * $P \leq 0.05$.

(C) ECs were transduced with myc-tagged PAK3 and fibronectin fibrillogenesis was quantified by isolating DOC-insoluble fibronectin and western blotting. Conversely, overexpression of PAK3 significantly increased fibrillogenesis (means ± SEM; n=3 independent experiments). * $P \leq 0.05$.

(D) ECs were transduced with either GFP, GFP-RhoJ QL or GFP-Cdc42 QL. Binding partners of active RhoJ and Cdc42 were determined by GFP-Trap and TMT mass spectrometry (see Data S2). The table shows the subset of previously identified Cdc42 binding partners and the

ratio of their abundance compared to the GFP control. The abundance ratios of RhoJ compared to the GFP control are shown too. RhoJ showed reduced binding to Cdc42 effectors such as SPEC2 and BORG2. PAK3 was the shared effector with the highest binding to RhoJ.

(E) The ability of PAK3 to rescue RhoJ-mediated inhibition of fibrillogenesis was investigated by transducing ECs with combinations of the active RhoJ mutant and PAK3. Fibronectin fibrillogenesis was assessed by quantifying DOC-insoluble fibronectin as before. Fibrillogenesis was also examined by immunofluorescence microscopy (Figure S3G). Expression of PAK3 partially rescued the RhoJ-mediated suppression of fibrillogenesis. By corollary, expression of RhoJ QL inhibited the promotion of fibrillogenesis by PAK3 (means ± SEM; n=3 independent experiments). * $P \leq 0.05$.

(F) Immunohistochemistry was performed on whole mount retina from littermate control $RhoJ^{WT/WT}$ mice and the RhoJ null $RhoJ^{GFP/GFP}$ mice on postnatal day 7 (P7). Staining was undertaken using rat anti-PECAM-1(red; to mark the retinal vessels) and mouse anti-EDA-fibronectin antibodies (green; clone IST-9). The lower panel represents a zoomed in image of the angiogenic front. See also Figure S4E. Scale bars: Top panel = 200μm; bottom panel = 20μm.

STAR★METHODS

LEAD CONTACT AND MATERIALS AVAILABILITY

Further information and requests for resources and reagents should be directed to and will be fulfilled by the Lead Contact, Harry Mellor (h.mellor@bristol.ac.uk). All unique/stable reagents generated in this study are available from the Lead Contact without restriction.

EXPERIMENTAL MODEL AND SUBJECT DETAILS

Cell culture

Primary human umbilical vein endothelial cells (HUVEC) from pooled donors were from Lonza and were cultured at 37°C in complete endothelial cell growth media (EGM-2; Lonza) without VEGF. Cells were used between passages 2-6. Where indicated, HUVEC were transfected with siRNA oligonucleotides using GeneFECTOR lipid according to the manufacturer's protocol (Venn Nova). HEK 293T cells were cultured at 37°C in DMEM supplemented with 10% FBS, 100U/ml penicillin and 100μg/ml streptomycin.

Lentiviral transduction

Experiments used the lentiviral expression vector pLVXpuro vector (Takara Bio). Lentiviral particles were produced in a HEK293T packaging line, using standard methods. Briefly, cells were transfected with pLVXpuro and the packaging vectors pMDG2 and pAX2, using lipofectamine. After 48h, the culture supernatants were added to ECs for 6h. Cells were selected for stable expression in media supplemented with 2μg/ml puromycin.

RhoJ KO mice

The generation of *Rhoj*$^{GFP/GFP}$ mice was described previously [5]. To obtain *RhoJ*$^{GFP/GFP}$ mice and littermate control *RhoJ*$^{WT/WT}$ mice, heterozygous *Rhoj*$^{GFP/WT}$ male and female with a C57BL/6 background were intercrossed. Both males and females were included since no differences between sexes were observed. Mice were healthy with normal immune status, were not subject to prior procedures, were fed with unlimited access to food and water, and were housed in specific pathogen-free condition. Animal care and all experimental procedures were performed under the approval by the Animal Experimentation Committee of Osaka University.

METHOD DETAILS

Immunofluorescence microscopy

ECs were fixed in 4% paraformaldehyde and permeabilized with 0.2% Triton X-100 or 0.1% saponin, as indicated. Confocal microscopy was performed using a Leica SP5 AOBS confocal laser-scanning microscope with an attached Leica DM I6000 inverted microscope. Confocal sections were taken across the z-plane and processed to form a 2D projection representing the full depth of the cell culture.

Vesicle isolation and proteomics

The protocol for vesicle enrichment and sorting was adapted from [35]. Briefly, ECs transduced with GFP-RhoJ QL were washed with ice-cold PBS and scraped into homogenization buffer (250mM sucrose, 8mM $CaCl_2$, 4mM $MgCl_2$, 78mM KCl, 10mM EGTA, 5mM HEPES, pH 7.2 with protease inhibitors). The cells were homogenized in a Balch homogenizer with a tungsten carbide ball bearing (10μm clearance). Homogenates were centrifuged for 5min at 1000 x *g* to remove the nuclei. The post-nuclear supernatant was loaded on top of a 10-30% iodixanol density gradient and ultracentrifugation was carried out for 18h at 4°C. Endosomal fractions were post-labelled with Calcein Violet-AM [12] and sorted using a Becton Dickinson Influx high speed sorter custom configured for small particle detection and sorting. Protein from GFP/Calcein double-positive vesicles was precipitated with TCA and the pellet was washed three times with ice-cold acetone and resuspended in SDS-PAGE sample buffer. Samples were run approximately 1cm into the separating gel and the gel lane was then cut as a single gel slice and subjected to in-gel tryptic digestion. The resulting peptides were fractionated using an Ultimate 3000 nanoHPLC system in line with an LTQ-Orbitrap Velos mass spectrometer (Thermo Scientific). The raw data files were processed and quantified using Proteome Discoverer software v1.4 (Thermo Scientific) and searched against the UniProt Human database using the SEQUEST algorithm. Peptide precursor mass tolerance was set at 10ppm, and MS/MS tolerance was set at 0.8Da. Search criteria included carbamidomethylation of cysteine (+57.0214) as a fixed modification and oxidation of methionine (+15.9949) as a variable modification. Searches were performed with full tryptic digestion and a maximum of 1 missed cleavage was allowed. The reverse database search option was enabled, and all peptide data were filtered to satisfy a false discovery rate of 1%.

Immunoprecipitation

ECs were washed with ice-cold PBS and harvested in lysis buffer (20 mM Tris pH7.5, 137 mM NaCl, 0.5% NP-40, 2mM sodium orthovanadate, 10mM sodium fluoride) containing protease inhibitor cocktail. Cell lysates were centrifuged for 12min at 12,000 x g at 4ºC. The clarified supernatants were incubated with the relevant antibodies for 30min and the complexes captured by subsequent incubation for 2h with Protein G Sepharose beads (Sigma-Aldrich). The beads were washed 3 times in lysis buffer and the immunoprecipitated proteins were then extracted from the beads by heating at 95°C with SDS-PAGE sample buffer, prior to analysis by western blotting. For immunoprecipitation of GFP-tagged proteins, lysates were incubated directly with GFP-Trap A beads (ChromoTek).

Cell adhesion assays

96 well cell culture plates were coated with either BSA (3%), fibronectin (2μg/ml), collagen I (2 μg/ml) or purified basement membrane (10% Geltrex). 6000 ECs were seeded per well and allowed to adhere for 15min. The unattached cells were removed with PBS. Attached cells were fixed with glutaraldehyde, stained with DAPI and counted using the Incucyte automated imaging system (Sartorius).

Quantification of fibronectin fibrillogenesis

Fibronectin fibrillogenesis was quantified by immunofluorescence microscopy and analysis of DOC-insoluble fibronectin. For quantification by immunofluorescence microscopy, 1 x 10^5 HUVEC cells were plated on coverslips in a 12-well plate. After 24h, cells were fixed with 4% PFA and stained for EDA-fibronectin. Images were acquired using a 40x oil lens on a Leica DMI6000 inverted epifluorescence microscope. 15 random fields were acquired per condition. Fibers were identified using ImageJ with the Ridge Detection plugin with width estimation enabled. Fibril density (pixels positive for objects identified as fibres) was calculated using a custom macro. Alternatively, ECs were incubated with 2.5μg/ml soluble rhodamine fibronectin (Cytoskeleton Inc) for 30min at 37ºC followed by fixation. The rhodamine fibronectin incorporated into fibrillar structures was imaged by widefield microscopy and the intensity of staining was quantified using ImageJ. Quantification of deoxycholate-insoluble fibronectin was performed as previously described [25][25][25][25]. Briefly, 2x10^5 ECs were plated in 6-well tissue culture dishes and cultured for 24h. Cells were washed with ice-cold PBS and lysed in 500μl of lysis buffer (20mM Tris, pH 8.5, 1% sodium deoxycholate, 2mM iodoacetamide, 2mM EDTA and protease inhibitors). Lysates were centrifuged at 20,000 x *g* for 30min to sediment the DOC-insoluble material. The resulting pellets were then washed twice more with lysis buffer and analyzed by western blotting.

To quantify secreted fibronectin, ECs were washed and incubated with fresh, serum free EGM-2 for 24 h. After media collection, the samples were diluted 10-fold to measure fibronectin concentrations within the linear range, using a Quantikine ELISA kit (R&D Systems) according to manufacturer's instructions. The amount of secreted fibronectin was calculated from a standard curve of known concentrations of pure fibronectin.

Integrin internalization assays

Integrin internalization assays were adapted from [36]. Briefly, ECs were grown to confluency, washed twice with cold PBS, and surface-labelled on ice with 0.2mg/ml cleavable biotin (NHS-SS-biotin; Pierce) in serum-free DMEM for 30min. Cells were then transferred to 37ºC to allow for internalization of surface-labelled proteins. At each time point, cells were returned to ice, washed twice with cold PBS and biotin was removed from proteins remaining at the surface using the reducing agent, MesNa (2.9mg/ml for 30min at 4ºC). Free sulfhydryl groups were alkylated with iodoacetamide to prevent further biotinylation. The amount of internalized biotinylated integrin α5β1 and active α5β1 were measured by capture-ELISA using Maxisorp (Nunc) plates coated with monoclonal antibodies recognizing total α5β1 or active α5β1 heterodimer (SNAKA51).

Integrin recycling assays

Integrin recycling assays were adapted from [36]. Briefly, following surface labeling with cleavable biotin, cells were transferred to serum-free DMEM for 30min at 37ºC to allow internalization. Cells were then washed twice with ice-cold PBS, and biotin was removed from proteins remaining at the cell surface using reduction with MesNa. The internalized fraction was then chased by returning the cells to 37°C in serum-free DMEM for the time points indicated. At each time point, the cells were returned to ice and biotin label was removed by a second round of MesNa treatment. The remaining biotinylated, internal integrin was quantified by capture ELISA.

Surface biotinylation assay

ECs were transfected with siRNAs, as before. After 48h, the cells were washed twice with ice-cold PBS, and surface-labelled on ice with 0.2mg/ml non-cleavable biotin (Sulfo-NHS-LC-Biotin, Pierce) for 30min. Cells were washed in ice-cold PBS, lysed and the biotinylated proteins captured on streptavidin agarose beads. The unbound fraction (the internal pool) and the captured fraction (surface pool) were evaluated by immunoblotting.

TMT mass spectrometry

ECs were transduced with GFP, GFP-RhoJ QL or GFP Cdc42 QL. Each condition used two confluent 10cm tissue culture dishes. GFP-tagged proteins were isolated from cell lysates using GFP-Trap A beads, as before. After the washes, the immunoprecipitated samples were reduced (10mM TCEP 55°C, 1h), alkylated (18.75mM iodoacetamide, room temperature, 30min) and digested on the beads with trypsin (2.5μg trypsin; 37°C, overnight), then labelled with Tandem Mass Tag (TMT) six plex reagents according to the manufacturer's protocol (ThermoFisher Scientific). The labelled samples were pooled prior to analysis by nano-LC MSMS using an Orbitrap Fusion Tribrid Mass Spectrometer. The raw data files were processed and quantified using Proteome Discoverer software v2.1 (Thermo Scientific) and searched against the UniProt Human database using the SEQUEST algorithm. Peptide precursor mass tolerance was set at 10ppm, and MS/MS tolerance was set at 0.6Da. Search criteria included oxidation of methionine (+15.9949) as a variable modification and carbamidomethylation of cysteine (+57.0214) and the addition of the TMT mass tag (+229.163) to peptide N-termini and

lysine as fixed modifications. Searches were performed with full tryptic digestion and a maximum of 2 missed cleavages were allowed. The reverse database search option was enabled, and all data were filtered to satisfy a false discovery rate of 5%.

Immunohistochemistry

The procedures for preparations of retinal samples have been described previously [37]. The primary antibodies were rat anti-CD31 (1:500, Mec13.3, BD Biosciences), and mouse anti-fibronectin (1:200, IST-9, Santa Cruz Biotechnology). Signals were detected with donkey IgGs conjugated with Alexa Fluor 568 or Alexa Fluor 647 (Life Technologies). Images of a retinal quadrant were taken with an LSM710 confocal microscope and combined using photomerge utility of Photoshop CS5 Extended software (version 12.0, Adobe).

QUANTIFICATION AND STATISTICAL ANALYSIS

Statistical analysis was performed using Graphpad Prism software. One-sample t-test was used to compare fold changes against the normalized control in experiments comparing 2 samples. In experiments with 3 or more samples with a single independent variable, one-way repeat measures ANOVA (block ANOVA) was used followed by Dunnett's multiple comparisons test. In experiments with 2 independent variables (Figures 2F, G), two-way repeat measures ANOVA (block ANOVA) was used followed by Bonferroni's multiple comparisons test. *** $P \leq 0.001$; ** $P \leq 0.01$; * $P \leq 0.05$.

DATA AND CODE AVAILABILITY

Custom macros for fibronectin fibrillogenesis analysis are freely available from the sources listed in the Key Resources Table.

SUPPLEMENTARY DATA LEGENDS

Data S1. RhoJ vesicle proteomics, related to Figure 1

RhoJ+ vesicles were purified by fluorescence activated vesicle sorting (FAVS) and mass spectrometry as described in STAR methods. The proteome was analyzed in Proteome Discoverer v1.4 and those satisfying 1% False Detection Rate cut off are represented in the Excel file. Column A, (Accession) is the unique identifier assigned to the protein by the FASTA database. Column B (Description) is the name of the protein. Column C (Score) is the protein score which is the sum of all scores for individual peptides. A score for a peptide is the sum of Xcorr values above the specified threshold. The score threshold is calculated as follows: 0.8 + peptide_charge × peptide_relevance_factor where peptide_relevance_factor is used at a default value of 0.4. For each spectrum, only the highest-scoring match is used. Column D (Coverage)

is the percentage of protein sequence covered by the identified peptides. Column E (#Unique peptides) displays the number of peptides unique to the protein group. Column F (#Peptides) displays the number of distinct peptide sequences in the protein group. Column G (#PSMs) displays the total number of identified peptide sequences (peptide spectrum matches) for the protein, including those redundantly identified. Column H (Area) displays the average area of the three unique peptides with the largest peak area.

Data S2. Comparative interactomes of RhoJ and Cdc42, related to Figure 4
GFP Trap Immunoprecipitation followed by TMT Mass spectrometry was performed as described in the STAR methods. The Excel file shows the proteins identified at 5% False discovery rate (FDR). Abundances are a measure of the reporter ions generated from the tandem mass tags at MS3. The raw abundance values for the 3 conditions GFP control, GFP RhoJ-QL and GFP Cdc42-QL IPs are represented (columns C to E). The raw abundances are normalized to the GFP abundances in each case to obtain interactor abundances normalized to the amount of RhoJ and Cdc42 immunoprecipitated (column F to H). The RhoJ-QL/GFP control and Cdc42-QL/GFP control values represent the fold enrichment of the interacting protein over GFP only control (Abundance ratios-column I and J).

REFERENCES

1. Ridley, A.J. (2015). Rho GTPase signalling in cell migration. Curr Opin Cell Biol *36*, 103-112.
2. Boureux, A., Vignal, E., Faure, S., and Fort, P. (2007). Evolution of the Rho family of ras-like GTPases in eukaryotes. Mol Biol Evol *24*, 203-216.
3. Kaur, S., Leszczynska, K., Abraham, S., Scarcia, M., Hiltbrunner, S., Marshall, C.J., Mavria, G., Bicknell, R., and Heath, V.L. (2011). RhoJ/TCL regulates endothelial motility and tube formation and modulates actomyosin contractility and focal adhesion numbers. Arterioscler Thromb Vasc Biol *31*, 657-664.
4. Yuan, L., Sacharidou, A., Stratman, A.N., Le Bras, A., Zwiers, P.J., Spokes, K., Bhasin, M., Shih, S.C., Nagy, J.A., Molema, G., et al. (2011). RhoJ is an endothelial cell-restricted Rho GTPase that mediates vascular morphogenesis and is regulated by the transcription factor ERG. Blood *118*, 1145-1153.
5. Kim, C., Yang, H., Fukushima, Y., Saw, P.E., Lee, J., Park, J.S., Park, I., Jung, J., Kataoka, H., Lee, D., et al. (2014). Vascular RhoJ is an effective and selective target for tumor angiogenesis and vascular disruption. Cancer Cell *25*, 102-117.
6. Takase, H., Matsumoto, K., Yamadera, R., Kubota, Y., Otsu, A., Suzuki, R., Ishitobi, H., Mochizuki, H., Kojima, T., Takano, S., et al. (2012). Genome-wide identification of endothelial cell-enriched genes in the mouse embryo. Blood *120*, 914-923.
7. Eelen, G., Dubois, C., Cantelmo, A.R., Goveia, J., Brüning, U., DeRan, M., Jarugumilli, G., van Rijssel, J., Saladino, G., Comitani, F., et al. (2018). Role of glutamine synthetase in angiogenesis beyond glutamine synthesis. Nature *561*, 63-69.

8. Shi, T.T., Li, G., and Xiao, H.T. (2016). The Role of RhoJ in Endothelial Cell Biology and Tumor Pathology. Biomed Res Int *2016*, 6386412.
9. Richards, M., Hetheridge, C., and Mellor, H. (2015). The Formin FMNL3 Controls Early Apical Specification in Endothelial Cells by Regulating the Polarized Trafficking of Podocalyxin. Curr Biol *25*, 2325-2331.
10. Barry, D.M., Xu, K., Meadows, S.M., Zheng, Y., Norden, P.R., Davis, G.E., and Cleaver, O. (2015). Cdc42 is required for cytoskeletal support of endothelial cell adhesion during blood vessel formation in mice. Development *142*, 3058-3070.
11. Vignal, E., De Toledo, M., Comunale, F., Ladopoulou, A., Gauthier-Rouvière, C., Blangy, A., and Fort, P. (2000). Characterization of TCL, a new GTPase of the rho family related to TC10 andCcdc42. J Biol Chem *275*, 36457-36464.
12. Gray, W.D., Mitchell, A.J., and Searles, C.D. (2015). An accurate, precise method for general labeling of extracellular vesicles. MethodsX *2*, 360-367.
13. Francis, S.E., Goh, K.L., Hodivala-Dilke, K., Bader, B.L., Stark, M., Davidson, D., and Hynes, R.O. (2002). Central roles of alpha5beta1 integrin and fibronectin in vascular development in mouse embryos and embryoid bodies. Arterioscler Thromb Vasc Biol *22*, 927-933.
14. Bhaskar, V., Zhang, D., Fox, M., Seto, P., Wong, M.H., Wales, P.E., Powers, D., Chao, D.T., Dubridge, R.B., and Ramakrishnan, V. (2007). A function blocking anti-mouse integrin alpha5beta1 antibody inhibits angiogenesis and impedes tumor growth in vivo. J Transl Med *5*, 61.
15. Silva, R., D'Amico, G., Hodivala-Dilke, K.M., and Reynolds, L.E. (2008). Integrins: the keys to unlocking angiogenesis. Arterioscler Thromb Vasc Biol *28*, 1703-1713.
16. Moreno-Layseca, P., Icha, J., Hamidi, H., and Ivaska, J. (2019). Integrin trafficking in cells and tissues. Nat Cell Biol *21*, 122-132.
17. Bridgewater, R.E., Norman, J.C., and Caswell, P.T. (2012). Integrin trafficking at a glance. J Cell Sci *125*, 3695-3701.
18. Su, Y., Xia, W., Li, J., Walz, T., Humphries, M.J., Vestweber, D., Cabañas, C., Lu, C., and Springer, T.A. (2016). Relating conformation to function in integrin α5β1. Proc Natl Acad Sci U S A *113*, E3872-3881.
19. Clark, K., Pankov, R., Travis, M.A., Askari, J.A., Mould, A.P., Craig, S.E., Newham, P., Yamada, K.M., and Humphries, M.J. (2005). A specific alpha5beta1-integrin conformation promotes directional integrin translocation and fibronectin matrix formation. J Cell Sci *118*, 291-300.
20. Mana, G., Clapero, F., Panieri, E., Panero, V., Böttcher, R.T., Tseng, H.Y., Saltarin, F., Astanina, E., Wolanska, K.I., Morgan, M.R., et al. (2016). PPFIA1 drives active α5β1 integrin recycling and controls fibronectin fibrillogenesis and vascular morphogenesis. Nat Commun *7*, 13546.
21. Astrof, S., and Hynes, R.O. (2009). Fibronectins in vascular morphogenesis. Angiogenesis *12*, 165-175.
22. Mao, Y., and Schwarzbauer, J.E. (2005). Fibronectin fibrillogenesis, a cell-mediated matrix assembly process. Matrix Biol *24*, 389-399.
23. Zhou, X., Rowe, R.G., Hiraoka, N., George, J.P., Wirtz, D., Mosher, D.F., Virtanen, I., Chernousov, M.A., and Weiss, S.J. (2008). Fibronectin fibrillogenesis regulates three-dimensional neovessel formation. Genes Dev *22*, 1231-1243.
24. Shi, F., and Sottile, J. (2008). Caveolin-1-dependent beta1 integrin endocytosis is a critical regulator of fibronectin turnover. J Cell Sci *121*, 2360-2371.
25. Jones, M.C., Caswell, P.T., Moran-Jones, K., Roberts, M., Barry, S.T., Gampel, A., Mellor, H., and Norman, J.C. (2009). VEGFR1 (Flt1) regulates Rab4 recycling to control fibronectin polymerization and endothelial vessel branching. Traffic *10*, 754-766.

26. Kusuhara, S., Fukushima, Y., Fukuhara, S., Jakt, L.M., Okada, M., Shimizu, Y., Hata, M., Nishida, K., Negi, A., Hirashima, M., et al. (2012). Arhgef15 promotes retinal angiogenesis by mediating VEGF-induced Cdc42 activation and potentiating RhoJ inactivation in endothelial cells. PLoS One *7*, e45858.
27. Fukushima, Y., Okada, M., Kataoka, H., Hirashima, M., Yoshida, Y., Mann, F., Gomi, F., Nishida, K., Nishikawa, S., and Uemura, A. (2011). Sema3E-PlexinD1 signaling selectively suppresses disoriented angiogenesis in ischemic retinopathy in mice. J Clin Invest *121*, 1974-1985.
28. Ruiz, R., Jahid, S., Harris, M., Marzese, D.M., Espitia, F., Vasudeva, P., Chen, C.F., de Feraudy, S., Wu, J., Gillen, D.L., et al. (2017). The RhoJ-BAD signaling network: An Achilles' heel for BRAF mutant melanomas. PLoS Genet *13*, e1006913.
29. Zhang, L., and Elias, J.E. (2017). Relative Protein Quantification Using Tandem Mass Tag Mass Spectrometry. Methods Mol Biol *1550*, 185-198.
30. Kumar, R., Sanawar, R., Li, X., and Li, F. (2017). Structure, biochemistry, and biology of PAK kinases. Gene *605*, 20-31.
31. Ho, H., Aruri, J., Kapadia, R., Mehr, H., White, M.A., and Ganesan, A.K. (2012). RhoJ regulates melanoma chemoresistance by suppressing pathways that sense DNA damage. Cancer Res *72*, 5516-5528.
32. Arjonen, A., Alanko, J., Veltel, S., and Ivaska, J. (2012). Distinct recycling of active and inactive β1 integrins. Traffic *13*, 610-625.
33. Simons, M. (2012). An inside view: VEGF receptor trafficking and signaling. Physiology (Bethesda) *27*, 213-222.
34. Urner, S., Planas-Paz, L., Hilger, L.S., Henning, C., Branopolski, A., Kelly-Goss, M., Stanczuk, L., Pitter, B., Montanez, E., Peirce, S.M., et al. (2019). Identification of ILK as a critical regulator of VEGFR3 signalling and lymphatic vascular growth. EMBO J *38*.
35. Cho, Y.G., Choi, B.J., Kim, C.J., Song, J.H., Zhang, C., Nam, S.W., Lee, J.Y., and Park, W.S. (2008). Genetic analysis of the DBC2 gene in gastric cancer. Acta Oncol *47*, 366-371.
36. Roberts, M., Barry, S., Woods, A., van der Sluijs, P., and Norman, J. (2001). PDGF-regulated rab4-dependent recycling of alphavbeta3 integrin from early endosomes is necessary for cell adhesion and spreading. Curr Biol *11*, 1392-1402.
37. Uemura, A., Ogawa, M., Hirashima, M., Fujiwara, T., Koyama, S., Takagi, H., Honda, Y., Wiegand, S.J., Yancopoulos, G.D., and Nishikawa, S. (2002). Recombinant angiopoietin-1 restores higher-order architecture of growing blood vessels in mice in the absence of mural cells. J Clin Invest *110*, 1619-1628.

KEY RESOURCES TABLE

REAGENT or RESOURCE	SOURCE	IDENTIFIER
Antibodies		
Mouse monoclonal anti-RhoJ	Abnova	Cat# H00057381-M01; RRID:AB_426036
Rabbit monoclonal anti-Na^+/K^+ ATPase α1 (D4Y7E)	Cell Signaling Technologies	Cat# 23565; RRID:AB_2798866
Rabbit monoclonal anti-EEA1	Cell Signaling Technologies	Cat# 3288; RRID:AB_2096811
Goat polyclonal anti-CD63	Santa Cruz Biotechnology	Cat# sc-7080; RRID:AB_648167
Rabbit anti-LAMP-1 (270c)	gift from Prof. Ash Toye	NA
Rabbit polyclonal anti-LAMP2	Thermo Fisher Scientific	Cat# PA1-655; RRID:AB_2134625
Mouse monoclonal anti-calnexin	BD Biosciences	Cat# 610523; RRID:AB_397883
Mouse monoclonal anti-integrin α5 (CD49e)	BD Biosciences	Cat# 610633; RRID:AB_397963
Mouse monoclonal anti-integrin α5β1 (Clone VC5)	BD Biosciences	Cat# 555651; RRID:AB_396007
Mouse monoclonal anti-integrin β1	DSHB	Cat# p5d2; RRID:AB_528308
Mouse monoclonal anti-PECAM	R&D Systems	Cat# BBA7, RRID:AB_356960
Mouse monoclonal anti- α-tubulin, ascites fluid, clone B-5-1-2	Sigma Aldrich	Cat#T5168; RRID:AB_477579
Mouse monoclonal anti-active integrin α5β1 (SNAKA51)	Novus Biologicals	Cat# NBP250146
Sheep polyclonal anti-TGN46	Serotec	Cat# AHP500GT, RRID:AB_2203291
Mouse monoclonal anti-fibronectin (IST-9). Raised	Santa Cruz Biotechnology	Cat# sc-59826, RRID:AB_783389

against the EDA domain of fibronectin		
Mouse monoclonal anti-fibronectin (FN-3E2). Raised against the EDA domain of fibronectin	Sigma Aldrich	Cat# 6140
Rabbit polyclonal anti-fibronectin	Proteintech	Cat# 15613-1-AP, RRID:AB_2105691
Rabbit polyclonal anti-vimentin	Proteintech	Cat# 10366-1-AP, RRID:AB_2273020
Mouse monoclonal anti-Cdc42	BD Biosciences	Cat# 610928, RRID:AB_398243
Rabbit polyclonal anti-PAK3	Cell Signaling Technologies	Cat# 2609, RRID:AB_2225298
Rabbit polyclonal anti-GFP	Cell Signaling Technologies	Cat# 2555, RRID:AB_10692764
Mouse monoclonal anti-myc-epitope tag (9E10)	Santa Cruz Biotechnology	Cat# sc-40, RRID:AB_627268
Chemicals, Peptides, and Recombinant Proteins		
FRAX 486	R&D Systems	Cat# 5190
Rhodamine-fibronectin	Cytoskeleton, Inc	Cat# FNR01-A
Fibronectin	Sigma Aldrich	Cat# F0895
Collagen I	Advanced Biomatrix	Cat# 5409
GFP-trap agarose beads	Chromotek	Cat# gta-20
Myc-trap agarose beads	Chromotek	Cat# yta-20
EZ-Link Sulfo NHS-LC-Biotin	Thermo Fisher	Cat# 21335
Sulfo-NHS-SS-Biotin	Thermo Fisher	Cat# PG82077
Human Fibronectin Quantkine ELISA kit	R&D Biosystems	Cat# DFBN10
Experimental Models: Cell Lines		

Human umbilical vein endothelial cells (HUVEC) from pooled donors	Lonza	Cat# C2519A
Experimental Models: Organisms/Strains		
RhoJ WT mice	Generated in [5]	C57BL/6 background
Rhoj$^{GFP/GFP}$ GFP knock-in null mice	Generated in [5]	C57BL/6 background
Oligonucleotides		
Mission siRNA Universal Negative Control	Sigma Aldrich	Cat#SIC001-5X1NMOL
siRNA targeting PAK3 (siPAK3-1) GACAAGAGGUGGCCAUAAA	Dharmacon	MU-003614-00- 0002 (siGenome Set of 4)
siRNA targeting PAK3 (siPAK3-2) GGAUGGCUCUGUUAAAUUG	Dharmacon	MU-003614-00- 0002 (siGenome Set of 4)
siRNA targeting RhoJ (siRhoJ-1) CCACUGUGUUUGACCACUATT	This paper	Eurofins
siRNA targeting RhoJ (siRhoJ-2) AGAAACCUCUCACUUACGATT	This paper	Eurofins
siRNA targeting Cdc42 (siCdc42-1) CUAUGCAGUCACAGUUAUGTT	This paper	Eurofins
siRNA targeting Cdc42 (siCdc42-2) CAUGUCUCCUGAUAUCCUATT	This paper	Eurofins

Recombinant DNA		
Plasmid pEGFP-Cdc42 Cdc42 with N-terminal GFP tag	This paper	NA
Plasmid pEGFP-RhoJ RhoJ with N-terminal GFP tag	This paper	NA
Plasmid pEGFP Cdc42-QL Constitutively-active Cdc42 (Q61>L) with N-terminal GFP tag	This paper	NA
Plasmid pEGFP RhoJ QL Constitutively-active RhoJ (Q79>L) with N-terminal GFP tag	This paper	NA
pLVx-puro GFP Cdc42QL Lentiviral expression vector encoding constitutively-active Cdc42	This paper	NA
pLVx puro GFP RhoJ-QL Lentiviral expression vector encoding constitutively-active RhoJ	This paper	NA
pLVx puro Myc PAK3 Lentiviral expression vector encoding myc-tagged PAK3	This paper	NA
Software and Algorithms		
Proteome Discoverer 2.1	Thermo Scientific	manufacturer
ImageJ	[35]	https://imagej.nih.gov/ij/
MIA workflow plugin	This paper	https://github.com/SJCross/MIA/tree/v0.9.22
Ridge detection plugin for ImageJ	Github	https://github.com/thorstenwagner/ij-ridgedetection/tree/v1.4.0

Figure 1

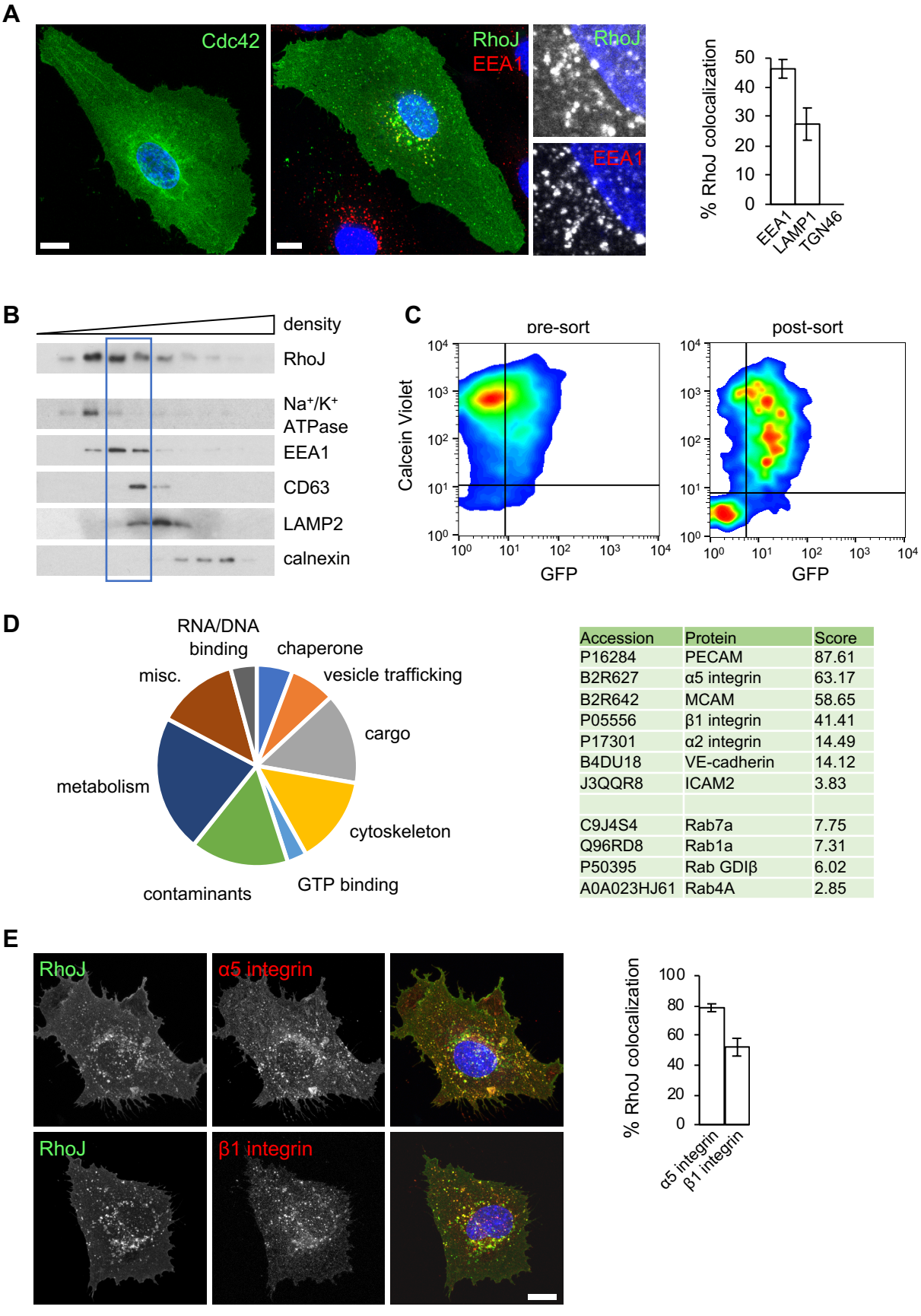

Accession	Protein	Score
P16284	PECAM	87.61
B2R627	α5 integrin	63.17
B2R642	MCAM	58.65
P05556	β1 integrin	41.41
P17301	α2 integrin	14.49
B4DU18	VE-cadherin	14.12
J3QQR8	ICAM2	3.83
C9J4S4	Rab7a	7.75
Q96RD8	Rab1a	7.31
P50395	Rab GDIβ	6.02
A0A023HJ61	Rab4A	2.85

Figure 2

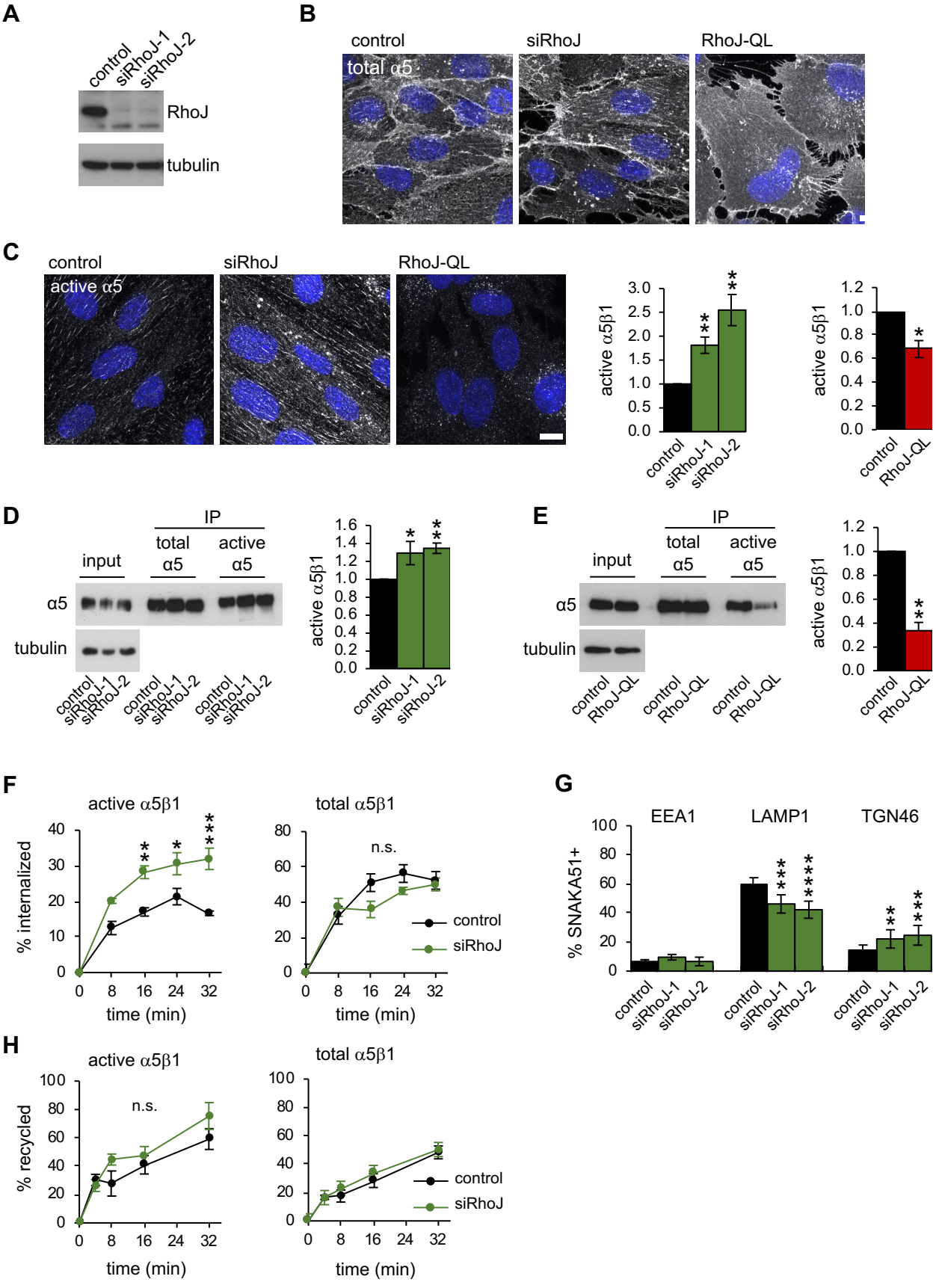
A
control
siRhoJ-1
siRhoJ-2
RhoJ
tubulin
B
control
siRhoJ
RhoJ-QL
total α5
C
control
siRhoJ
RhoJ-QL
active α5
active α5β1
control
siRhoJ-1
siRhoJ-2
control
RhoJ-QL
D
IP
input
total α5
active α5
α5
tubulin
active α5β1
E
F
active α5β1
total α5β1
% internalized
time (min)
n.s.
control
siRhoJ
G
EEA1
LAMP1
TGN46
% SNAKA51+
H
% recycled

Figure 3

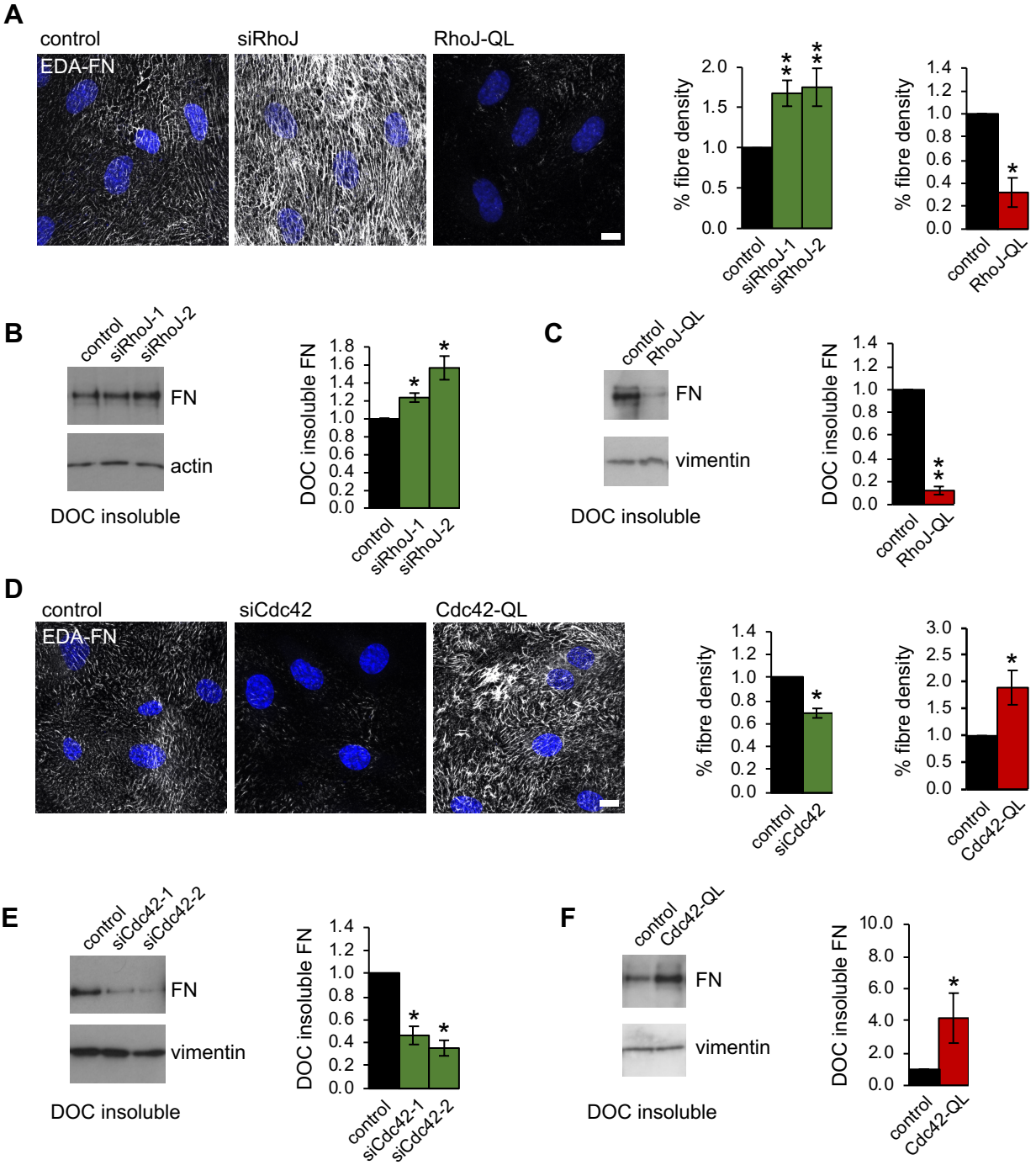
A
control
siRhoJ
RhoJ-QL
EDA-FN
% fibre density
control
siRhoJ-1
siRhoJ-2
RhoJ-QL
B
FN
actin
DOC insoluble
DOC insoluble FN
C
vimentin
D
siCdc42
Cdc42-QL
siCdc42
E
siCdc42-1
siCdc42-2
F

Figure 4

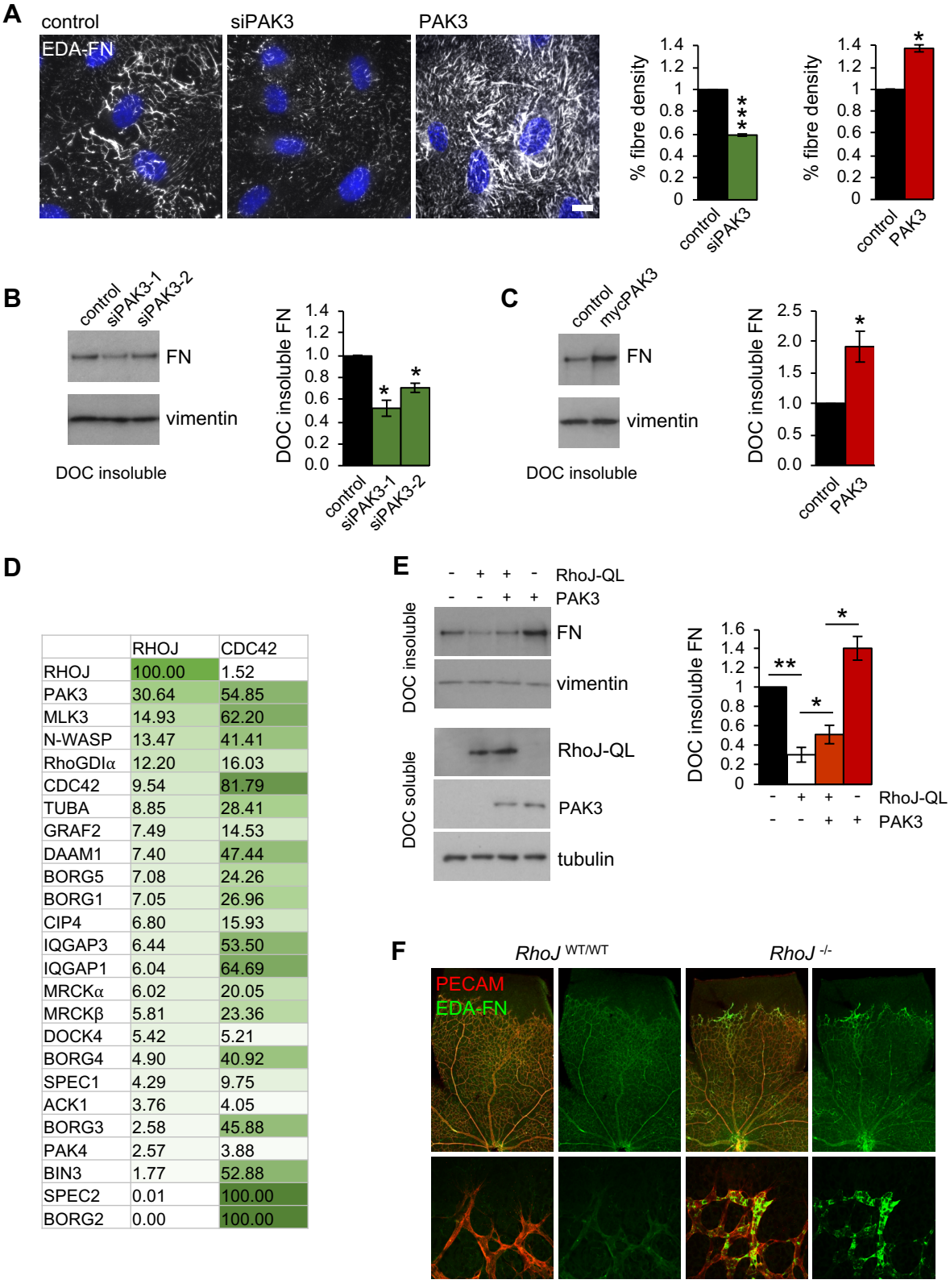

	RHOJ	CDC42
RHOJ	100.00	1.52
PAK3	30.64	54.85
MLK3	14.93	62.20
N-WASP	13.47	41.41
RhoGDIα	12.20	16.03
CDC42	9.54	81.79
TUBA	8.85	28.41
GRAF2	7.49	14.53
DAAM1	7.40	47.44
BORG5	7.08	24.26
BORG1	7.05	26.96
CIP4	6.80	15.93
IQGAP3	6.44	53.50
IQGAP1	6.04	64.69
MRCKα	6.02	20.05
MRCKβ	5.81	23.36
DOCK4	5.42	5.21
BORG4	4.90	40.92
SPEC1	4.29	9.75
ACK1	3.76	4.05
BORG3	2.58	45.88
PAK4	2.57	3.88
BIN3	1.77	52.88
SPEC2	0.01	100.00
BORG2	0.00	100.00

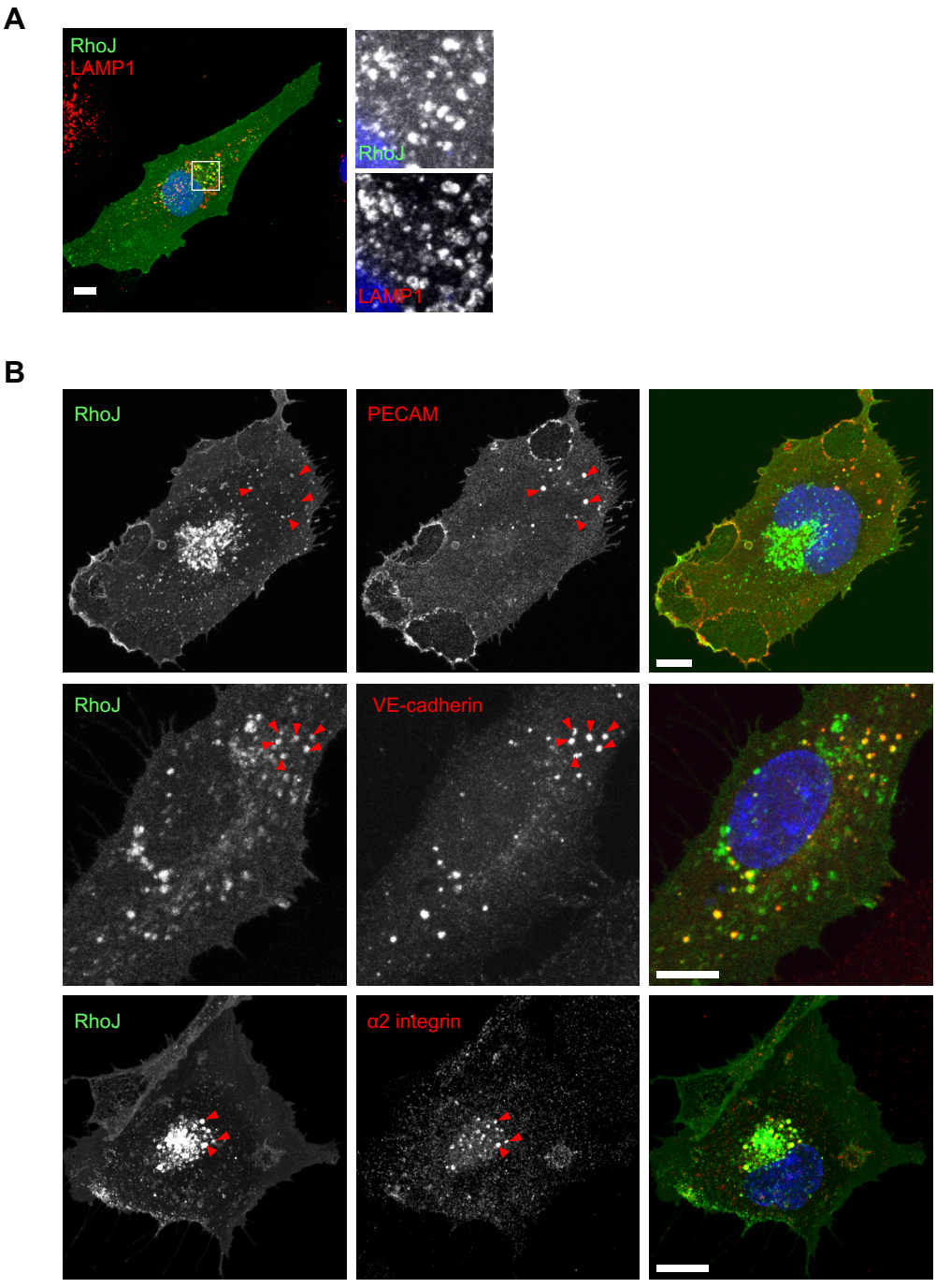
A
RhoJ
LAMP1
RhoJ
LAMP1
B
RhoJ
PECAM
RhoJ
VE-cadherin
RhoJ
α2 integrin

Figure S1. Endothelial RhoJ+ vesicles transport α5β1 integrin, related to Figure 1

(A) ECs were transfected with GFP-RhoJ. RhoJ was seen in vesicles that colocalized with EEA1 (Figure 1A) and with the late endosomal marker LAMP1 (red). Quantification is shown in Figure 1A. Scale bar = 10μm.

(B) ECs were transfected with GFP-RhoJ and co-stained for endogenous PECAM, VE-cadherin or integrin α2 (red). In each case, a subset of vesicles was positive for RhoJ (red arrowheads). Scale bar = 10μm.

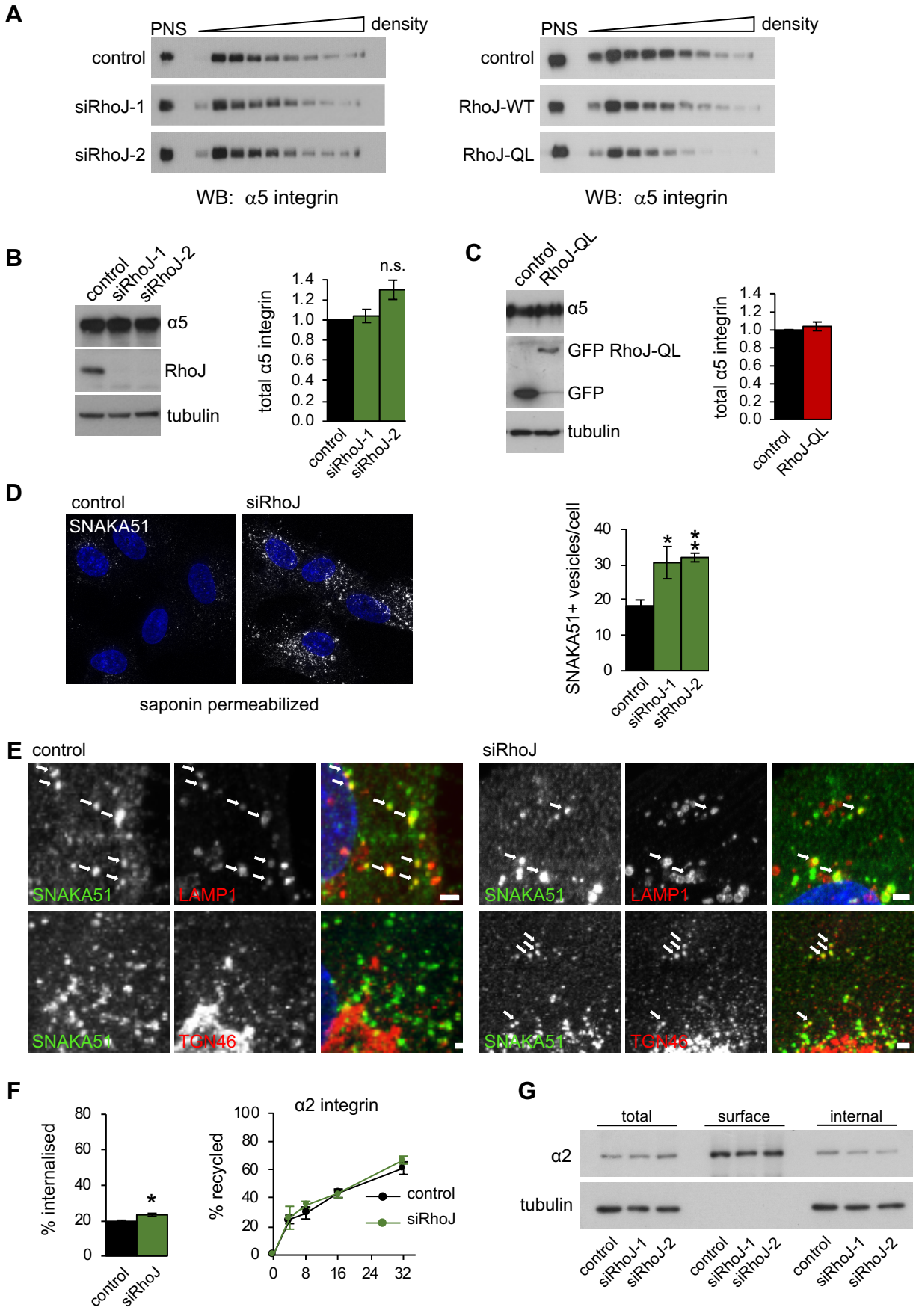
A
PNS
density
control
siRhoJ-1
siRhoJ-2
WB: α5 integrin
PNS
density
control
RhoJ-WT
RhoJ-QL
WB: α5 integrin
B
control
siRhoJ-1
siRhoJ-2
α5
RhoJ
tubulin
total α5 integrin
n.s.
control
siRhoJ-1
siRhoJ-2
C
control
RhoJ-QL
α5
GFP RhoJ-QL
GFP
tubulin
total α5 integrin
control
RhoJ-QL
D
control
siRhoJ
SNAKA51
saponin permeabilized
SNAKA51+ vesicles/cell
control
siRhoJ-1
siRhoJ-2
E
control
siRhoJ
SNAKA51
LAMP1
SNAKA51
TGN46
F
% internalised
control
siRhoJ
α2 integrin
% recycled
control
siRhoJ
G
total
surface
internal
α2
tubulin
control
siRhoJ-1
siRhoJ-2

Figure S2. RhoJ regulates active integrin α5β1 trafficking, related to Figure 2

(A) ECs were transfected with RhoJ siRNA or transduced with wild-type RhoJ (GFP-RhoJ-WT) or GFP-RhoJ-QL. Postnuclear supernatants (PNS) were subjected to density gradient ultracentrifugation on 10-30% iodixanol gradients. The cellular distribution of α5 integrin was analyzed by western blotting. Neither silencing of RhoJ, or expression of the wild type or activated RhoJ affected α5 integrin distribution.

(B) ECs were treated ± RhoJ siRNA and total α5 integrin was quantified by western blotting. Data are means ± SEM; n=3 independent experiments. Silencing of RhoJ had no effect on total α5 integrin levels.

(C) ECs were transduced with activated RhoJ and total α5 integrin was quantified by western blotting. Data are means ± SEM; n=3 independent experiments. Expression of activated RhoJ had no effect on total α5 integrin levels.

(D) ECs were treated ± RhoJ siRNA and cells were fixed and permeabilized with saponin to selectively reveal SNAKA51+ vesicles. The number of SNAKA51+ vesicles per cell was increased significantly on silencing of RhoJ. Data are means ± SEM; n=6 independent experiments, with 5 cells quantified per experiment for each condition.

(E) ECs were treated ± RhoJ siRNA. After 48h, the steady-state distribution of active α5β1 integrin was determined by confocal immunofluorescence microscopy. Representative confocal images with active α5β1 in green and the compartment markers LAMP1 and TGN46 (red) are shown. Arrows indicate colocalization. Silencing of RhoJ decreased colocalization of active α5β1 with LAMP1+ vesicles and increased colocalization with TGN46+ vesicles (see Figure 2G). Scale bar = 2μm.

(F) ECs were treated ± RhoJ siRNA. After 72h, cells were surface biotinylated on ice and then allowed to internalize surface proteins at 37°C for 24min. Biotin on the remaining non-internalized receptors was then removed using MesNa on ice. The amount of internalized α2 integrin is shown as a percentage of the initial surface pool. Silencing of RhoJ caused a small but significant increase in the rate of internalization of α2 integrin. The internalized pool was then chased over the time points indicated and the biotin from recycled receptors was again removed by reduction with MesNa on ice. The amount of internalized pool lost to the surface is represented as % of the initial internalized pool in each case. Silencing of RhoJ had no significant effect on the recycling rate for total α2β1. Data are means ± SEM; n=3 experiments. * $P \leq 0.05$.

(G) ECs were treated ± RhoJ siRNA. After 48h, surface proteins were biotinylated on ice. The cells lysates were incubated with streptavidin beads to capture surface proteins and the unbound fraction was taken as the internal pool. The surface and internal pools of α2 integrin were then examined by western blotting. There was no apparent effect of RhoJ depletion on the surface or internal levels of α2 integrin.

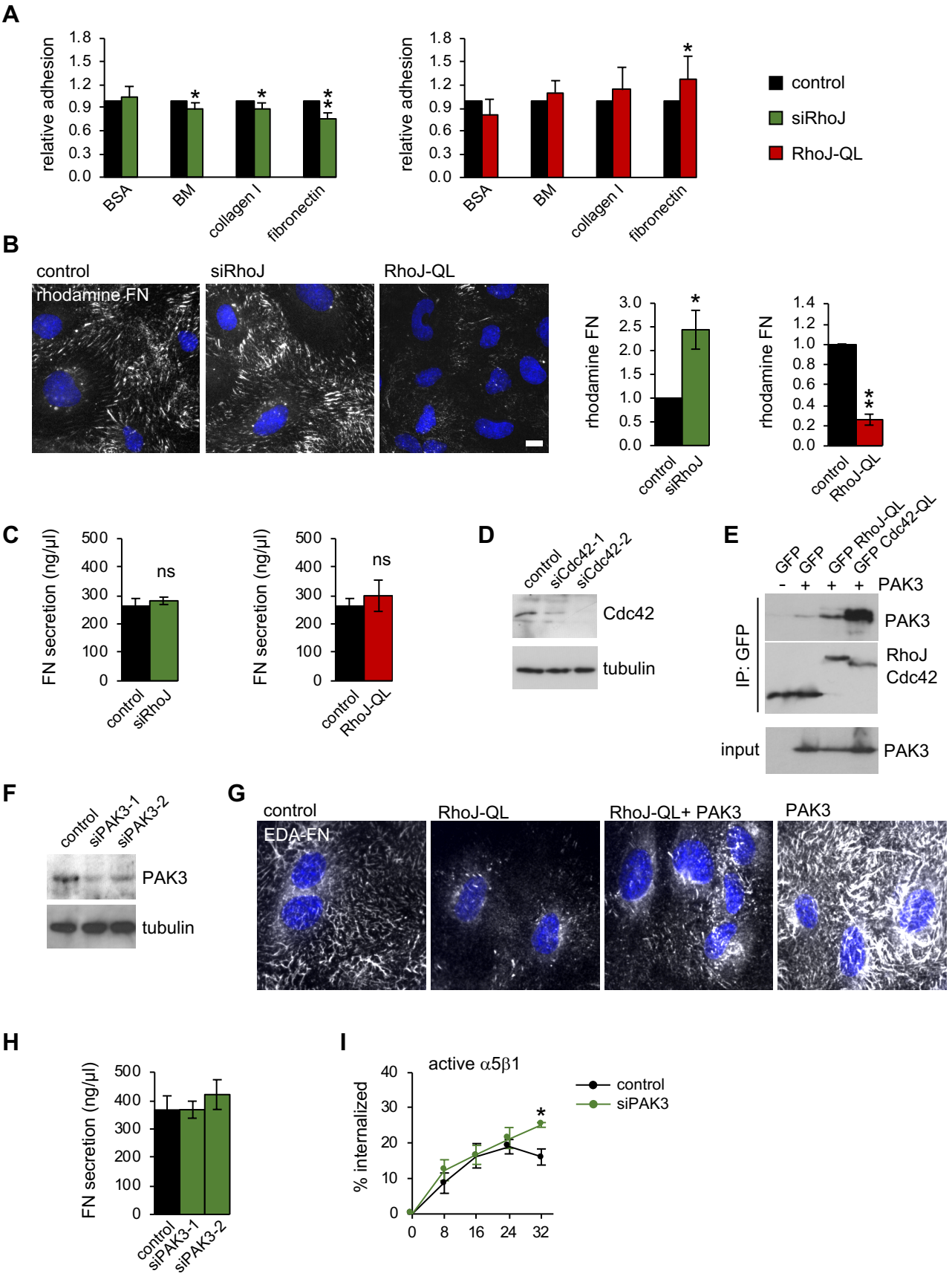
A
relative adhesion
1.8
1.5
1.2
0.9
0.6
0.3
0.0
BSA
BM
collagen I
fibronectin
control
siRhoJ
RhoJ-QL
B
control
siRhoJ
RhoJ-QL
rhodamine FN
rhodamine FN
3.0
2.5
2.0
1.5
1.0
0.5
0.0
control
siRhoJ
1.4
1.2
1.0
0.8
0.6
0.4
0.2
0.0
control
RhoJ-QL
C
FN secretion (ng/µl)
500
400
300
200
100
0
ns
control
siRhoJ
control
RhoJ-QL
D
control
siCdc42-1
siCdc42-2
Cdc42
tubulin
E
GFP
GFP
GFP RhoJ-QL
GFP Cdc42-QL
PAK3
IP: GFP
PAK3
RhoJ
Cdc42
input
PAK3
F
control
siPAK3-1
siPAK3-2
PAK3
tubulin
G
control
EDA-FN
RhoJ-QL
RhoJ-QL+ PAK3
PAK3
H
FN secretion (ng/µl)
500
400
300
200
100
0
control
siPAK3-1
siPAK3-2
I
active α5β1
% internalized
40
30
20
10
0
0
8
16
24
32
control
siPAK3

Figure S3. RhoJ regulates the endothelial assembly of fibrillar fibronectin, related to Figure 3

(A) ECs were treated ± RhoJ siRNA or transduced with activated RhoJ-QL. Cells were plated in triplicate onto the indicted ECM components or a BSA control. After 15min, adherent cells were then fixed and counted. Cells depleted of RhoJ showed a small but significant decrease in adhesion to all ECM components. Cells expressing activated RhoJ showed a small but significant increase in adhesion to all ECM components. Data are means ± SEM; n=6 independent experiments). * $P \leq 0.05$.

(B) ECs were treated ± RhoJ siRNA or transduced with activated RhoJ-QL and then incubated with 2.5 µg/ml rhodamine fibronectin for 30min. Scale bar = 10µm. The intensity of signal per cell was quantified from 10 random widefield images per condition. Silencing of RhoJ significantly increased the deposition of fibronectin. Expression of activated RhoJ decreased fibronectin deposition. Data are means ± SEM; n=5 independent experiments. ** $P \leq 0.01$; * $P \leq 0.05$.

(C) ECs were transfected with siRNA targeting RhoJ or transduced with activated RhoJ-QL. Cell medium was conditioned for 24h and the amount of fibronectin secreted by cells was determined by ELISA. Depletion of RhoJ had no effect on fibronectin secretion. Data are means ± SEM; n=3 independent experiments.

(D) ECs were transfected with two independent siRNAs targeting Cdc42 and the effectiveness of silencing determined by western blotting.

(E) HEK 293T cells were transiently transfected with combinations of PAK3, RhoJ-QL and Cdc42-QL, as indicated. Cdc42 and RhoJ were isolated by GFP-Trap immunoprecipitation and the coimmunoprecipitation of PAK3 was determined by western blotting. Both RhoJ and Cdc42 interacted with PAK3; however, the association of PAK3 with activated Cdc42 was greater.

(F) ECs were transfected with two independent siRNAs targeting PAK3 and the effectiveness of silencing determined by western blotting.

(G) The ability of PAK3 to rescue RhoJ-mediated inhibition of fibrillogenesis was investigated by transducing ECs with combinations of the active RhoJ mutant and PAK3. Expression of PAK3 partially rescued the RhoJ-mediated suppression of fibrillogenesis. By corollary, expression of RhoJ QL inhibited the promotion of fibrillogenesis by PAK3. Fibronectin fibrillogenesis was assessed by quantifying DOC-insoluble fibronectin (Figure 4E).

(H) ECs were transfected with siRNAs targeting PAK3 or a control. Cell medium was conditioned for 24h and the amount of fibronectin secreted by cells was determined by ELISA. Depletion of PAK3 had no effect on fibronectin secretion. Data are means ± SEM; n=3 independent experiments.

(I) ECs were treated ± PAK3 siRNA. After 72h, cells were surface biotinylated on ice and then allowed to internalize surface proteins at 37°C. At each timepoint, the remaining surface biotinylation was removed by MesNa treatment, and the amount of internalized active α5β1 integrin was determined by streptavidin capture of biotinylated proteins and ELISA with specific antibodies. Silencing of PAK3 had no significant effect on the internalization of total α5β1 integrin, but significantly increased lifetime of the internalized integrin. Data are means ± SEM; n=3 independent experiments. * $P \leq 0.05$.

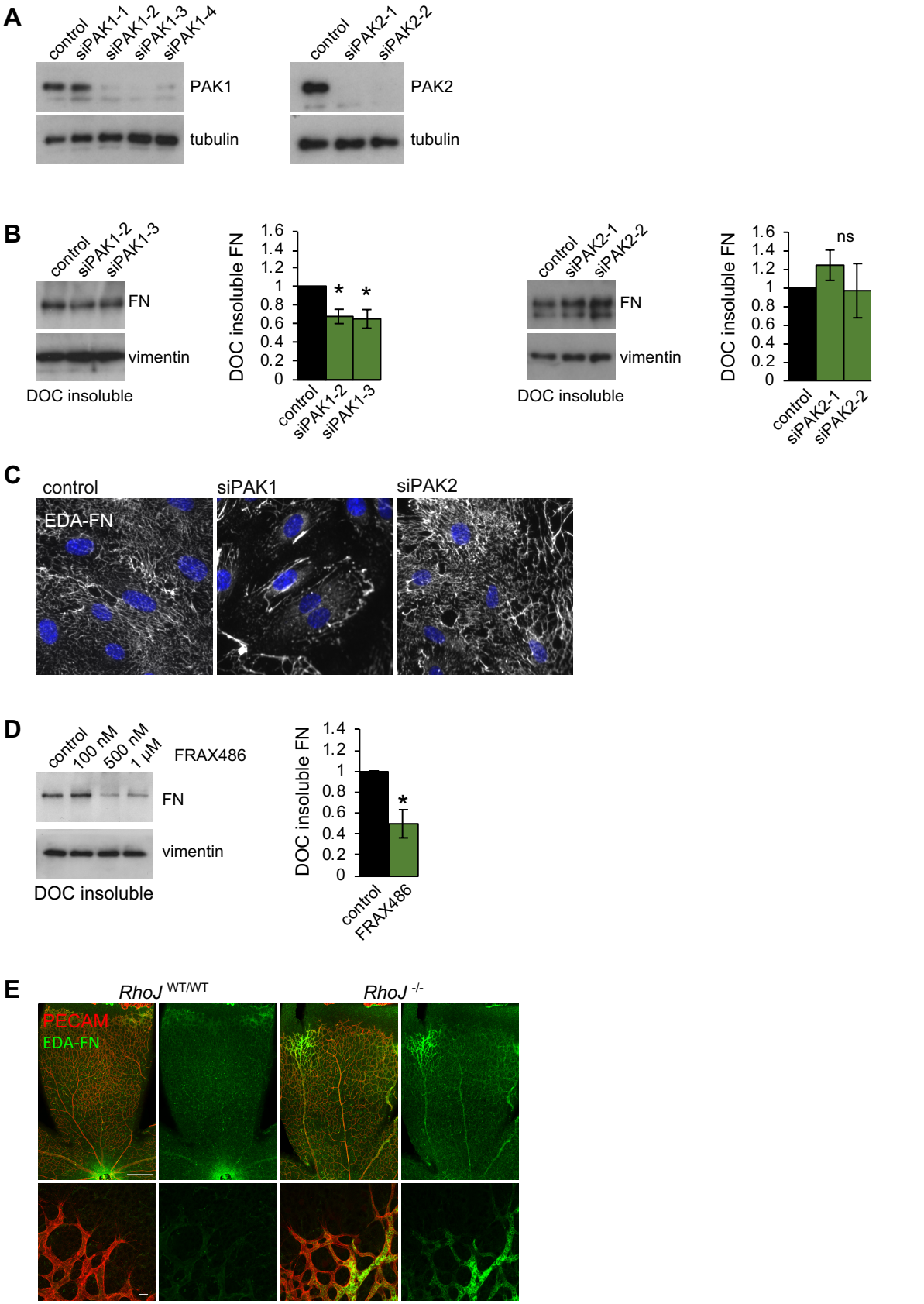
A
control
siPAK1-1
siPAK1-2
siPAK1-3
siPAK1-4
PAK1
tubulin
control
siPAK2-1
siPAK2-2
PAK2
tubulin
B
control
siPAK1-2
siPAK1-3
FN
vimentin
DOC insoluble
DOC insoluble FN
control
siPAK1-2
siPAK1-3
control
siPAK2-1
siPAK2-2
FN
vimentin
DOC insoluble
DOC insoluble FN
ns
control
siPAK2-1
siPAK2-2
C
control
siPAK1
siPAK2
EDA-FN
D
control
100 nM
500 nM
1 µM
FRAX486
FN
vimentin
DOC insoluble
DOC insoluble FN
control
FRAX486
E
RhoJ WT/WT
RhoJ -/-
PECAM
EDA-FN

Figure S4. RhoJ opposes Cdc42 in endothelial fibronectin fibrillogenesis through competition for PAK3, related to Figure 4

(A) ECs transfected with siRNAs targeting PAK1 and PAK2 and their ability to silence expression of the proteins was assessed after 48h by western blotting.

(B) Fibronectin fibrillogenesis in ECs was quantified by isolating deoxycholate (DOC) insoluble fibronectin and western blotting. Silencing of PAK1 significantly decreased fibrillogenesis while PAK2 had no effect. Data are means ± SEM; n=3 independent experiments. * $P \leq 0.05$.

(C) ECs were treated ± siRNA targeting PAK1 or PAK2. Fibronectin deposition was examined by staining cells with an EDA-fibronectin antibody to detect cell-secreted fibronectin specifically. Silencing of PAK2 had no apparent effect on fibronectin fibrillogenesis; however, silencing of PAK1 dramatically reduced fibril formation

(D) ECs were treated with the Group I PAK inhibitor, FRAX486 at the concentrations indicated. Fibronectin fibrillogenesis was quantified by isolating deoxycholate (DOC) insoluble fibronectin and western blotting. The effects of treatment with 500 nM FRAX486 were quantified. Inhibition of Group I PAKs reduced fibronectin fibrillogenesis by 50%. Data are means ± SEM; n=3 independent experiments. * $P \leq 0.05$.

(E) Immunohistochemistry was performed on whole mount retina from littermate control $RhoJ^{WT/WT}$ mice and the RhoJ null $RhoJ^{GFP/GFP}$ mice on postnatal day 7 (P7). Staining was undertaken using rat anti-PECAM-1(red; to mark the retinal vessels) and mouse anti-EDA-fibronectin antibodies (green; clone 3E2). The lower panel represents a zoomed in image of the angiogenic front. See also Figure 4F. Scale bars: Top panel = 200μm; bottom panel = 20μm.